Chemically Enhancing Block Copolymers for Block-Selective Synthesis of Self-Assembled Metal Oxide Nanostructures

Jovan Kamcev,[†] David S. Germack,[‡] Dmytro Nykypanchuk,[†] Robert B. Grubbs,[†] Chang-Yong Nam,[†,*] and Charles T. Black[†,*]

[†]Center for Functional Nanomaterials and [‡]Condensed Matter Physics and Materials Science Department, Brookhaven National Laboratory, Upton, New York 11973, United States

ABSTRACT

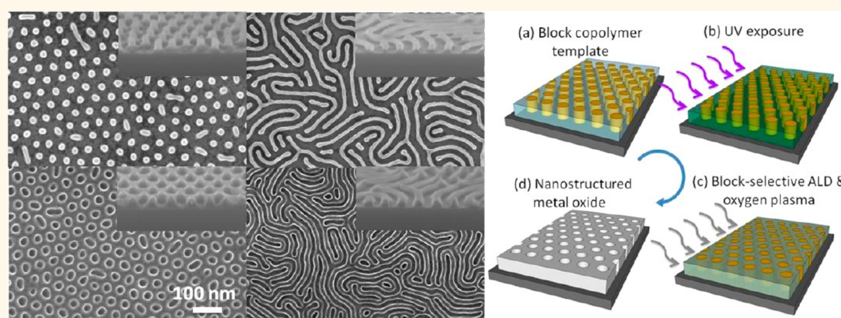

We report chemical modification of self-assembled block copolymer thin films by ultraviolet light that enhances the block-selective affinity of organometallic precursors otherwise lacking preference for either copolymer block. Sequential precursor loading and reaction facilitate formation of zinc oxide, titanium dioxide, and aluminum oxide nanostructures within the polystyrene domains of both lamellar- and cylindrical-phase modified polystyrene-*block*-poly(methyl methacrylate) thin film templates. Near-edge X-ray absorption fine structure measurements and Fourier transform infrared spectroscopy show that photo-oxidation by ultraviolet light creates Lewis basic groups within polystyrene, resulting in an increased Lewis base—acid interaction with the organometallic precursors. The approach provides a method for generating both aluminum oxide patterns and their corresponding inverses using the same block copolymer template.

KEYWORDS: block copolymers · infiltration synthesis · atomic layer deposition · metal oxides · photo-oxidation

Thin films of diblock copolymers are useful for self-assembly-based patterning materials due to their ease of processing and ability to spontaneously form dense, uniform nanometer-scale features over arbitrarily large areas.[1,2] The assembly process is driven by molecular interactions, as the copolymer consists of two immiscible polymer blocks bound together by a covalent bond. Pattern formation results as the material phase-separates to minimize its free energy, with the nanostructure geometry and dimensions tunable through adjustment of the copolymer molecular weight and constituent block weight ratio.[3−5]

Phase-separated block copolymer films can be used as photoresist substitutes for lithographic patterning,[1,6−12] and they have also found application as nanometer-scale reactors for controlled synthesis of inorganic materials.[13−20] For example, some early research using block copolymers for lithography used block-selective staining with OsO_4 for imaging purposes and also to improve the material's chemical etch resistance.[7] Likewise, metal nanoparticles can be positioned on surfaces through preferential interaction with one of the phase-separated block copolymer domains.[21−23] A new scheme for selectively loading copolymer domains with organometallic precursors and

* Address correspondence to cynam@bnl.gov, ctblack@bnl.gov.

Received for review September 6, 2012 and accepted December 19, 2012.

Published online December 19, 2012
10.1021/nn304122b

© 2012 American Chemical Society

reaction to form metal oxides shows promise for enabling further applications of these materials.[17,18,24−27] This idea, termed sequential infiltration synthesis, builds upon the approaches of area-selective chemical vapor deposition[6] and area-selective atomic layer deposition.[28]

Sequential infiltration synthesis proceeds by exposure of self-assembled polystyrene-*block*-poly(methyl methacrylate) (PS-*b*-PMMA) thin films to vapors of specific organometallic precursors (*e.g.*, trimethylaluminum (TMA) or titanium tetrachloride), selected for their ability to perfuse the film and selectively bind only to PMMA through a strong attractive interaction with its ester carbonyl groups. The process relies on selective precursor attachment to PMMA during the first growth cycle. The precursors are converted to metal oxides by sequential exposure to water vapor, and the grown inorganic material provides reactive sites for subsequent growth cycles. Removal of the polymer template after growth results in a metal oxide having features replicating the dimensions and geometry of the initial PMMA domain. PS-*b*-PMMA block copolymers are well suited for implementing this scheme, but with only a limited number of organometallic precursors. Growth of materials from organometallic precursors without a suitable PMMA attachment chemistry (*e.g.*, diethylzinc (DEZ) for ZnO, tri(*tert*-pentoxy)silanol for SiO_2, and tungsten hexafluoride for W) can be initiated by first seeding the PMMA with one cycle of a different material suitable for block-selective growth (*e.g.*, Al_2O_3).[18] Meanwhile, developing new block copolymer material systems tailored for selective attraction with specific organometallic precursors represents a significant undertaking.

In this work, we demonstrate an approach to chemically modifying PS-*b*-PMMA thin films to enhance their ability to selectively localize weakly interacting organometallic precursors. Specifically, we photo-oxidize the PS domain by ultraviolet (UV) light irradiation and create nanostructured metal oxides (such as ZnO and TiO_2) that reflect dimensions of the PS domain—in contrast to the typical case in which the PMMA domain acts as the nucleation site for metal oxide growth. Using near-edge X-ray absorption fine structure (NEXAFS) and Fourier transform infrared (FTIR) spectroscopies, we measure UV-induced formation of oxygen-containing functional groups in the PS domain and suggest that its increased Lewis base−acid interaction with the organometallic precursors results in the switch of the primary metal oxide nucleation site. We also demonstrate a variation of the technique that creates both nanostructured metal oxide patterns and their inverses, using the identical starting block copolymer template.

RESULTS AND DISCUSSION

We form self-assembled PS-*b*-PMMA thin film templates using both cylindrical-phase (molecular weight M_n = 67 kg/mol, 70:30 PS/PMMA) and lamellar-phase

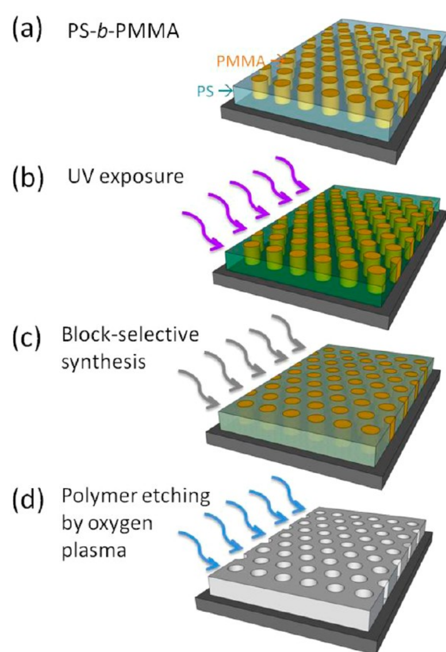

Scheme 1. Schematic description of the modified block-selective metal oxide synthesis. (a) Self-assembled PS-*b*-PMMA thin film on a Si substrate. A cylindrical phase is given as an example with light blue matrix and yellow cylinders indicating the PS and PMMA domains, respectively. (b) UV irradiation of the polymer template induces preferential chemical change (photo-oxidation) in the PS domain. (c) Block-selective growth of metal oxide by exposure to organometallic precursor/water atomic layer deposition cycles. (d) Removal of polymers by oxygen plasma etching reveals the nanopatterned metal oxide film resembling the dimension and geometry of the original PS domain.

(M_n = 75 kg/mol 50:50 PS/PMMA) materials (film thicknesses ∼30 nm) by spin-casting from toluene (1 wt %) onto Si substrates and thermal annealing at 205 °C for up to 5 h (in vacuum) (Scheme 1a). We promote perpendicular domain orientation in the copolymer layer by neutralizing the Si surface with a PS-*r*-PMMA random copolymer brush layer prior to application of the block copolymer film.[29] The resulting self-assembled cylindrical patterns consist of locally ordered hexagonal arrangements of cylindrical PMMA domains with ∼20 nm mean diameter, arranged with ∼40 nm average separation within a majority block PS matrix (Figure 1a). Lamellar materials generate fingerprint patterns of alternating PS and PMMA domains, with ∼40 nm pitch and roughly 50% duty cycle (Figure 1b).

Although DEZ is a widely used precursor for synthesis of ZnO films by chemical vapor deposition or atomic layer deposition, the material is known to interact only weakly with PS-*b*-PMMA, so that it is unsuited for block-selective synthesis of ZnO nanostructures unless the structure is first seeded by a different block-selective material.[18] Sequential exposure of cylindrical (Figure 1a) or lamellar (Figure 1b) PS-*b*-PMMA templates to six cycles of DEZ (1.3 Torr, 300 s) and water vapor (∼5 Torr, 300 s) results in only a random deposition of fine particles after polymer re-

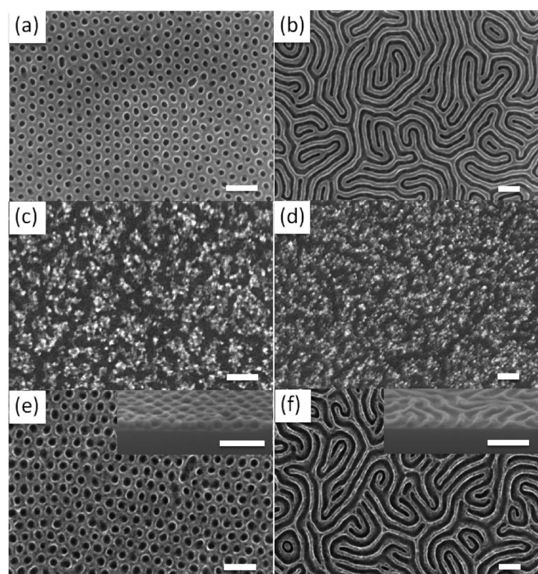

Figure 1. Scanning electron microscopy (SEM) micrographs showing self-assembled PS-*b*-PMMA thin film templates and corresponding nanostructured ZnO patterns created by block-selective growth using DEZ precursor. (a) Cylindrical and (b) lamellar patterns of the initial PS-*b*-PMMA templates. Here, PMMA domains were removed (appearing black) to enhance image contrast (see the Materials and Methods). (c,d) After six DEZ/water atomic layer deposition cycles on the unaltered control templates. Both (c) cylindrical and (d) lamellar templates show a random deposition of ZnO particles. (e,f) After six DEZ/water atomic layer deposition cycles on UV-irradiated PS-*b*-PMMA templates. Insets show 70° tilted cross-sectional views of the nanostructured ZnO patterns. Scale bars in all micrographs indicate 100 nm.

moval using oxygen plasma (Figure 1c,d). The resulting inorganic structures bear no resemblance to the initial polymer patterns, suggesting that there is little preferential attraction of DEZ to either PS or PMMA.

UV exposure of these same PS-*b*-PMMA block copolymer films under oxygen presence enhances the affinity between PS domains and weakly interacting organometallic precursors such as DEZ, enabling the block-selective growth of metal oxide nanostructures. After self-assembly by thermal annealing, we irradiate the polymer films with UV light (~0.8 mW/cm^2 low-pressure mercury lamp) in a N_2/O_2 (98/2) atmosphere for 5 min to chemically alter the polymer material (Scheme 1b). In contrast to the unexposed films, exposure of UV-irradiated PS-*b*-PMMA to six DEZ/water precursor cycles and following polymer removal by oxygen plasma (Scheme 1c,d) produces nanostructured ZnO patterns (Figure 1e,f) that are highly similar to the starting templates. Initial cylindrical PS-*b*-PMMA templates (Figure 1a) result in a ~24 nm thick ZnO film (thickness reduced by ~20% compared to the starting polymer template) fully perforated with holes having an average diameter of ~22 nm (~10% increase) and ~40 nm center-to-center spacing (unchanged, Figure 1e and inset). This confirms the selective infiltration of DEZ into the self-assembled PS domain, rather than precursor localization within PMMA domains as has been observed

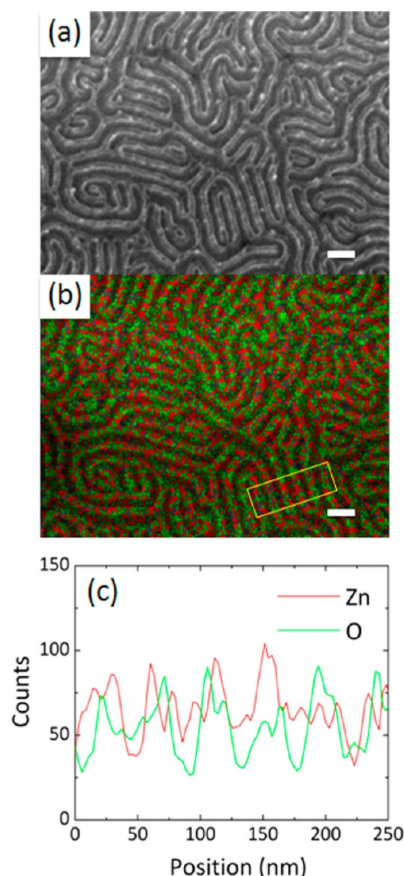

Figure 2. (a) SEM micrograph and (b) corresponding false-color-represented EDX mapping of the ZnO lamellar nanopattern created by six DEZ/water atomic layer deposition cycles on the UV-exposed self-assembled lamellar-phase PS-*b*-PMMA BCP template. In the EDX mapping, red and green denote Zn (K_α) and O (K_α), respectively. The corresponding EDX spectrum is shown in the Supporting Information (Figure S1). Scale bars indicate 100 nm. (c) Averaged EDX line scan intensity profile obtained in the yellow rectangular area in (b).

previously for organometallics such as TMA.[17,18] Similarly, lamellar-phase PS-*b*-PMMA templates (Figure 1b) generate ZnO striped patterns (Figure 1f) having ~21 nm line widths (nearly identical to the initial polymer template) and 40 nm repeat period (unchanged). Energy-dispersive X-ray spectroscopy (EDX) mapping of the striped pattern by scanning electron microscopy (SEM) (Figure 2) shows that the lamellar pattern contains Zn and O, consistent with the block-selective synthesis of ZnO.

UV exposure of PS qualitatively increases its affinity for attaching DEZ, while a similar exposure leaves the ability for PMMA to bind DEZ largely unchanged, as evidenced by ZnO infiltration synthesis performed on PS and PMMA homopolymer thin films in which only selected areas were UV-exposed using shadow masks. The UV-exposed PS homopolymer films nucleated growth of a continuous ZnO layer, compared to a layer of disconnected particles in unexposed sections (Supporting Information, Figure S2a,b). Both UV-exposed and unexposed

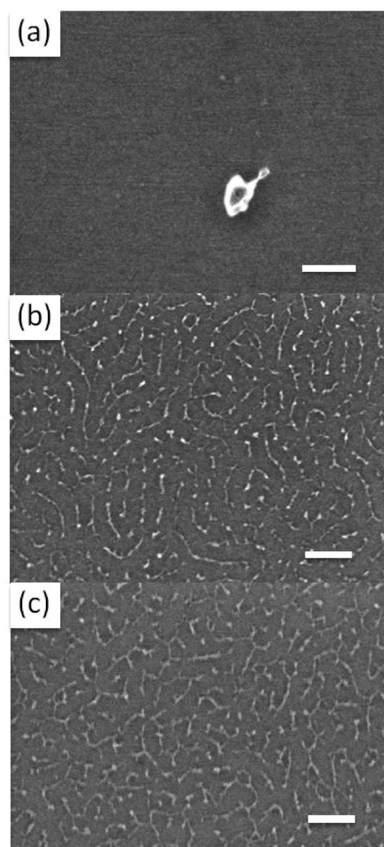

Figure 3. SEM micrographs of TiO_2 nanopatterns obtained after six TIP/water atomic layer deposition cycles on three different conditions of starting self-assembled PS-*b*-PMMA templates: (a) unaltered control lamellar pattern; (b) UV-exposed lamellar; (c) UV-exposed cylindrical. The polymers are removed by oxygen plasma etching after deposition. In (a), the lack of deposition created a featureless surface, while (b) and (c) display disconnected TiO_2 patterns. Scale bars indicate 100 nm.

PMMA homopolymer films nucleate disconnected ZnO particles, with a higher deposition density in unexposed sections (Figure S2c,d in Supporting Information). These experiments suggest that unexposed PMMA has a somewhat higher affinity for DEZ than unexposed PS, and that UV exposure renders PS more attractive to DEZ than PMMA.

Similarly to DEZ, titanium isopropoxide (TIP) is an organometallic precursor frequently used for thin film synthesis (of TiO_2) that we find is ill suited for block-selective synthesis within PS-*b*-PMMA domains. Exposure of an unmodified PS-*b*-PMMA film to six TIP/water cycles, followed by polymer removal using oxygen plasma, results in very little TiO_2 growth on the surface (Figure 3a), an indication that TIP interacts even more weakly with PS-*b*-PMMA than DEZ. The UV irradiation of the PS-*b*-PMMA film both increases the amount of synthesized TiO_2 and improves the fidelity of selective deposition (Figure 3b,c). While improved, the nanostructured TiO_2 patterns consist of disconnected particles only slightly resembling the initial polymer templates. This poor pattern formation is somewhat surprising since TIP is a stronger Lewis acid compared to DEZ, being often used in conjunction with chiral ligands as a catalyst for adding DEZ to aldehydes and ketones.[30] Given the larger molecular size of TIP compared to DEZ, we speculate that slower diffusion and subsequently lower sorption of TIP within the polymer domains may be the cause of poor deposition.[31] Nonetheless, the effect of UV-enhanced block selectivity of the organometallic precursor is evident in this case, as well.

We hypothesize that the substantial increase in block selectivity of weakly interacting organometallic precursors to the UV-irradiated PS-*b*-PMMA templates results from their enhanced Lewis acid−base interactions. Previous work has shown that certain organometallic precursors, such as DEZ, are weak Lewis acids, with little preferential affinity to ester groups (weak Lewis bases) within PMMA domains in PS-*b*-PMMA templates.[18] It is known that UV irradiation in the presence of oxygen introduces additional oxygen-containing functional groups through photo-oxidation, which changes material properties such as wettability and adhesiveness.[32,33] In PS-*b*-PMMA, UV irradiation readily decomposes the PS phenyl rings, creating hydroxyl, carboxyl, carbonate, and carbonyl groups,[34] each of which increases Lewis basicity compared to PS or PMMA. However, UV irradiation of PMMA induces chain scissions and removes ester groups, primarily resulting in formation of unsaturated carbon−carbon bonds that are weak Lewis bases.[35,36] Such UV-induced chemical modifications can preferentially increase Lewis basicity and complexing ability of the PS block with weak Lewis acid organometallic precursors. In light of this hypothesis, we conjecture that poor TiO_2 pattern formation using TIP could be improved using a $TiCl_4$ precursor because of its higher Lewis acidity[37] and strong affinity to oxygen-containing functional groups.[38] This observation is consistent with previous demonstrations of block-selective infiltration of TiO_2 using $TiCl_4$.[17]

NEXAFS spectroscopy provides a surface-sensitive probe of polymer oxidation[39] and confirms the UV-induced formation of oxygen-containing functional groups with stronger Lewis basicity within the PS domain. A comparison of measurements of a ∼20 nm thick UV-irradiated (5 min) PS film and an unaltered control sample (both spin-cast on Si substrates) shows the UV-induced formation of spectral peaks associated with the π^* orbital of C═O bonds ($\pi^*_{C=O}$, at photon energy ∼286.4 eV) (Figure 4a). The appearance of $\pi^*_{C=O}$ absorbances is accompanied by decreases in peak intensities for C═C and C−H bonds ($\pi^*_{C=C}$ at 285.1 eV and σ^*_{C-H} at 287.6 eV), consistent with photo-oxidation of the PS phenyl rings upon UV irradiation.[39]

NEXAFS spectra of UV-irradiated PS films are consistent with photo-oxidation proceeding from the top surface down through the film, similar to previous studies of PS photo-oxidation.[39,40] Decreasing the bias voltage of the electron yield detector during a NEXAFS

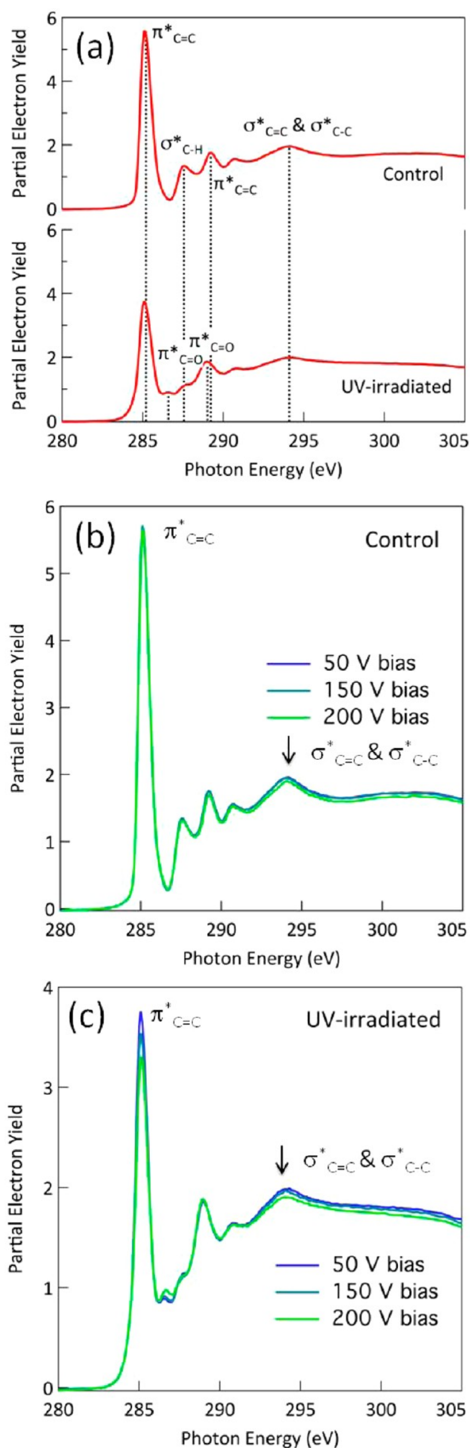

Figure 4. NEXAFS spectra of control and UV-irradiated PS thin film samples. (a) Control (top) *vs* UV-irradiated (bottom). (b,c) Detector bias-dependent variation of NEXAFS spectra (depth profiling) for (b) control and (c) UV-irradiated PS samples. Unlike the control PS sample that shows negligible bias dependence, the UV-irradiated sample displays appreciable decreases in $\pi^*_{C=C}$ and σ^*_{C-C} peaks with increasing bias voltage, indicating more significant oxidation toward the surface.

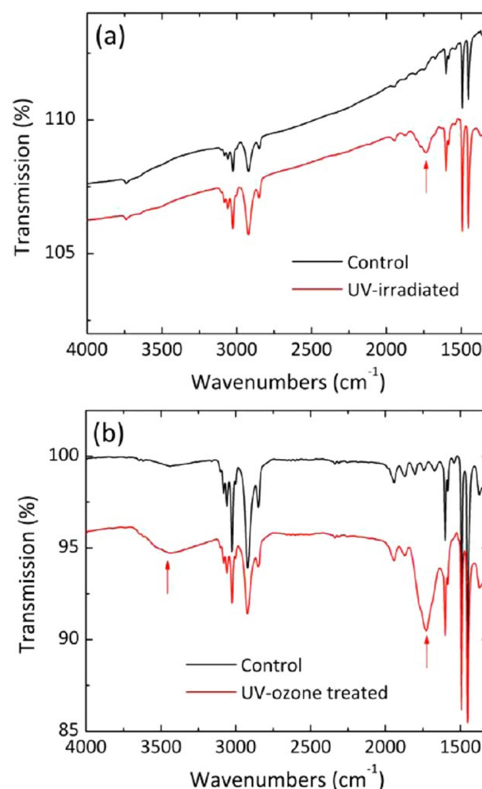

Figure 5. FTIR spectrum obtained from (a) drop-cast PS thin film samples before (black curve) and after (red curve) 60 min UV irradiation; (b) PS powder before (black) and after 60 min UV-ozone treatment (red) for extended oxidation. The new peaks around 1700 and 3200−3550 cm^{-1} (marked by red arrows) emerging after the oxidation are typically attributed to the carbonyl and hydroxyl groups, respectively.

measurement generally increases the collection of Auger electrons from deeper within the film,[39] ranging from the near-air surface (~1 nm) to several nanometers deep. While unaltered PS spectra show no bias dependence, characteristic of chemical homogeneity within the film (Figure 4b), the UV-irradiated PS sample displays decreases in $\pi^*_{C=C}$ and $\sigma^*_{C=CH}$ peak intensities near the surface (Figure 4c), a sign of more significant oxidation toward the surface.

FTIR spectroscopy provides further evidence for photo-oxidation of PS and formation of carbonyl, and potentially hydroxyl groups, within the PS domain during UV irradiation. We performed FTIR measurements using an attenuated total reflectance method with both film and powder samples. We drop-cast PS films (>1 μm thick) and then oxidized them by a 60 min UV exposure in order to enhance the FTIR signal (spin-cast thin film samples have an insufficient signal-to-noise ratio due to limited volume). The FTIR spectrum of the oxidized PS film (Figure 5a, red curve) possesses a broad absorbance band of the C═O stretching mode around 1700 cm^{-1}, which is absent in the unmodified PS sample (Figure 5a, black curve). This feature typically originates from the formation of oxygen-containing carbonyl groups such as aldehyde, ketone, and carboxyl groups, which exhibit stronger Lewis basicity compared to ester groups in unaltered PMMA.[41] The same absorbance feature appears more conspicuously when PS

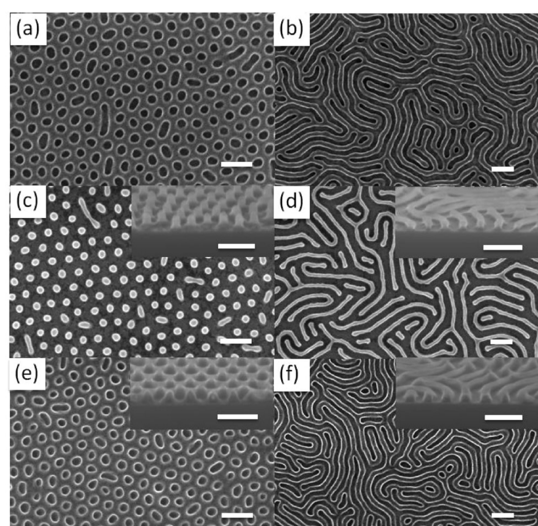

Figure 6. SEM micrographs showing self-assembled PS-*b*-PMMA thin film templates and corresponding nanostructured Al_2O_3 patterns created by block-selective deposition. (a) Cylindrical and (b) lamellar patterns of initial PS-*b*-PMMA templates with PMMA removed for the purpose of enhanced SEM contrast. (c,d) After three TMA/water atomic layer deposition cycles on unaltered (c) cylindrical- and (d) lamellar-phase templates, resulting in noninverted Al_2O_3 nanostructures grown on starting PMMA domains. (e,f) After six TMA/water atomic layer deposition cycles on UV-irradiated (e) cylindrical and (f) lamellar templates with PMMA domains removed prior to the deposition. Insets show the 70° tilted cross-sectional views. Polymers were removed by oxygen plasma etching after deposition. Scale bars in all images denote 100 nm.

powder samples are more extensively oxidized by 60 min UV-ozone treatment (Figure 5b), accompanied by the emergence of a broad absorbance near 3200–3550 cm^{-1}. The broad absorbances in this region are generally attributed to stretching of O–H bonds,[41] which can result from hydroxyl or carboxyl groups—another stronger Lewis base compared to the ester group in PMMA. We were unable to perform FTIR characterization of UV-exposed PS-*b*-PMMA thin films (~20 nm) because they provided an insufficient signal for meaningful analysis. However, FTIR analysis of thicker PS homopolymer films, coupled with NEXAFS spectroscopy of PS homopolymer thin films, provides strong evidence for photo-oxidation of the PS block in PS-*b*-PMMA templates by UV exposure.

Chemically enhancing the PS-*b*-PMMA template for block-selective synthesis allows us to generate nanostructured metal oxide patterns from either the PS domains or the PMMA domains of the same block copolymer template. For example, as has been previously reported, we can form nanostructured Al_2O_3 patterns by sequential exposure of unaltered cylindrical[17,18] or lamellar[25] PS-*b*-PMMA films (Figure 6a,b) to three TMA/water cycles. TMA is a strong Lewis acid compared to either DEZ or TIP and preferentially localizes within unaltered PMMA domains, resulting in nanostructured Al_2O_3 with dimensions and geometries similar to the PMMA template (Figure 6c,d). TMA also has a high affinity for hydroxyl and carbonyl/carboxyl groups created within PS domains by UV irradiation. Exposure of *UV-irradiated* PS-*b*-PMMA templates to the same three TMA/water cycles produces patterns inverted from the original, as the selective synthesis occurs within PS domains rather than within PMMA (Figure 6e,f). We note that after UV irradiation but prior to exposure to the organometallic precursors, we selectively removed the PMMA block using acetic acid and oxygen plasma[42] to prevent undesired continued block-selective attraction of TMA to the PMMA domain. The negligible deposition of Al_2O_3 in the open space between PS domains is due to the self-limiting characteristic of atomic layer deposition that only permits a monolayer deposition per cycle on a surface due to the removal of excess precursors by a purging step (*e.g.*, six ALD cycles of TMA should produce only ~0.6 nm thick Al_2O_3).[43] Without first removing PMMA domains, a majority of Al_2O_3 deposition still occurs in the PMMA, with deposition of fine Al_2O_3 particles on the PS domain (Figure S3 in Supporting Information), indicating still strong block-selective infiltration of TMA into the PMMA.

We understand this seemingly different interaction of TMA with the UV-exposed PS block in the polymer template, compared to DEZ and TIP, by considering the two underlying physical processes involved with block-selective infiltration: metal oxide precursor diffusion within the polymer film, and precursor attachment to functional groups within the polymer. Each with its own rate kinetics, an imbalance of the rates of these two processes *in either direction* would cause the infiltration synthesis to fail. For instance, little rate for precursor attachment to the functional groups in the polymer results in no metal oxide growth (as in DEZ or TIP's interaction with unexposed PS-*b*-PMMA). However, in the opposite extreme when the rate of attachment is much higher compared to the precursor diffusion rate, the result will be metal oxide growth only within a thin top surface layer of the polymer film. Further, this thin surface metal oxide layer will hinder precursor diffusion during following ALD cycles and only nucleate conventional ALD growth on the surface with deposition rate of a few angstroms per cycle at most. The result is then growth of a thin metal oxide layer (~1–2 nm) only on the surface of polymer template. Under this scenario, we hypothesize that UV exposure significantly increases the rate at which TMA binds to PS, such that the precursor binding and subsequent metal oxide formation become confined to the top surface of PS block—because TMA has a much higher Lewis acidity than DEZ,[44] and a stronger Lewis acid–base interaction between metal precursor and polymer template increases their binding reaction rate (similarly to organometallic reactions[45]), the UV-exposed PS can become too reactive for full film infiltration by TMA. Additionally, a thin Al_2O_3 layer formed only at the PS

surface under this case likely would not survive the O_2 plasma removal of the block copolymer, but the removal of the PMMA block prior to TMA exposure allows the precursor to infiltrate the PS domain from both top and sides, resulting perhaps in a more robust nanostructure. Such a conjecture requires further study, most directly by cross-sectional chemical analysis of the infiltrated PS domains, similar to previous investigations.[46]

CONCLUSION

Chemical modification of PS-*b*-PMMA block copolymer templates by UV-induced photo-oxidation enhances their ability for block-selective incorporation of organometallic precursors that otherwise lack a strong preferential attraction to either PS or PMMA. NEXAFS spectroscopy and FTIR measurements reveal that UV irradiation selectively creates oxygen-containing functional groups within the PS, enhancing Lewis base–acid interactions with otherwise weakly interacting organometallic precursor materials. This chemical modification allows formation of nanostructured ZnO and TiO_2 patterns, as well as Al_2O_3 patterns and their inverses using the same block copolymer template. These results not only expand the functionality of PS-*b*-PMMA template but also suggest a general strategy for developing and identifying new block copolymer materials (*e.g.*, polystyrene-*b*-poly(2-vinylpyridine) due to the high basicity of 2-vinylpyridine block) suitable for block-selective incorporation of a broader range of organometallic systems than currently possible.

MATERIALS AND METHODS

Materials. PS-*b*-PMMA block copolymers (M_n (kg/mol) = 46-*b*-21 (cylindrical phase); 38-*b*-37 (lamellar phase)) were purchased from Polymer Source, Inc. Hydroxy-terminated PS-*r*-PMMA (11 kg/mol)[29] was synthesized in the laboratory of Dr. Craig Hawker. Acetic acid (99%, ReagentPlus), acetone (HPLC grade), toluene (HPLC grade), and the organometallic precursors (DEZ, TIP, and TMA) were purchased from Sigma-Aldrich and used as received.

Preparation of PS-*b*-PMMA Templates. Si substrates were cleaned using an oxygen plasma (20 W, 100 mTorr, 5 min) in a reactive ion etcher (CS-1701, March Plasma, Inc.). PS-*r*-PMMA random copolymer (0.6 wt % in toluene) was deposited by spin-coating on the cleaned Si substrate at 750 rpm for 45 s using a spin-coater (Cee 200, Brewer Science). Films were annealed in a vacuum oven (Fisher Scientific) at 205 °C for 2 h. Annealed samples were rinsed with toluene to create a PS-*r*-PMMA brush. PS-*b*-PMMA films were deposited by spin-coating (from 1 wt % solution in toluene) on the random copolymer-treated Si substrate at 2000 rpm for 45 s, and the substrate was annealed in vacuum at 205 °C for up to 5 h.

Selective Removal of PMMA Domains. PMMA domains in the block copolymer patterns were selectively removed by exposing the film to UV light (generated by low pressure mercury lamp, ~0.8 mW/cm^2 measured by Oriel 70268 thermopile detector) for 5 min under flowing N_2, soaking in acetic acid for 3 min, followed by soaking in deionized water for 3 min, and a brief oxygen plasma etching (3–10 s, 20 W, 100 mTorr).

UV Irradiation of Block Copolymer Templates. Self-assembled templates were exposed to UV light (generated by low-pressure mercury lamp, ~0.8 mW/cm^2 measured by Oriel 70268 thermopile detector) for 5 min under flowing N_2/O_2 (98/2).

Block-Selective Synthesis of Metal Oxides. Block-selective synthesis of metal oxides was performed by exposure of PS-*b*-PMMA templates (either pristine or UV-irradiated) to between 3 and 6 precursor cycles using a Cambridge Nanotech Savannah S100 atomic layer deposition system (85 °C for TMA, 95 °C for DEZ, and 150 °C for TIP, with base pressure ~0.5 Torr). The sequential exposure cycle consisted of (a) 300 s exposure to organometallic precursor (DEZ, TIP, or TMA), (b) chamber purging by 100 sccm N_2 flow for 300 s, (c) 300 s exposure to water vapor. During the 300 s organometallic precursor exposure, the chamber pressure increased to different values depending on the type of precursor (DEZ ~1.3 Torr, TIP ~5 Torr, TMA ~6 Torr, water ~8 Torr). After the precursor exposure cycles, remaining polymer material was removed using an oxygen plasma (1 min, 20 W, 100 mTorr).

Characterization. The samples were characterized using a Hitachi S-4800 field emission SEM. EDX spectroscopy and elemental analysis were performed in a JEOL JSM-7600F field emission SEM equipped with an EDX detector. NEXAFS spectroscopy was performed at beamline U7A of the National Synchrotron Light Source at Brookhaven National Laboratory. Partial electron yield spectra of the carbon K-edge were collected with varying detector bias voltages as previously described.[39] The collected spectra were calibrated to a polyester calibration sample, normalized pre- and post-edge with respect to the beam current, and processed using a series of functions written for Igor Pro 6.2 (Wavemetrics Inc.) by Dr. Dean M. DeLonchamp of the National Institute of Standards and Technology. FTIR measurements were performed on spin-cast, drop-cast, and powdered PS samples under attenuated total reflectance mode using a Nicolet 6700 FTIR spectrophotometer equipped with single reflection ZnSe horizontal attenuated total reflectance accessory. The spin-cast sample (thickness ~20 nm) typically displayed a poor signal-to-noise ratio due to a limited sample volume. All measured samples were kept dry before measurements to eliminate the influence of water on the collected FTIR spectra.

Conflict of Interest: The authors declare no competing financial interest.

Acknowledgment. This research is supported by the U.S. Department of Energy, Basic Energy Sciences, at the Center for Functional Nanomaterials (J.K., D.N., R.B.G., C.-Y.N., and C.T.B.) and the Materials Sciences and Engineering Division (D.S.G.) (Contract No. DE AC02 98CH10886). This work was partially supported by the Energy Laboratory Research and Development Initiative at Brookhaven National Laboratory. The authors thank Dr. Mingzhao Liu for helpful discussion.

Supporting Information Available: Additional details and figures. This material is available free of charge *via* the Internet at http://pubs.acs.org.

REFERENCES AND NOTES

1. Black, C. T.; Ruiz, R.; Breyta, G.; Cheng, J. Y.; Colburn, M. E.; Guarini, K. W.; Kim, H. C.; Zhang, Y. Polymer Self Assembly in Semiconductor Microelectronics. *IBM J. Res. Dev.* **2007**, *51*, 605–633.
2. Segalman, R. A. Patterning with Block Copolymer Thin Films. *Mater. Sci. Eng. R* **2005**, *48*, 191–226.
3. Darling, S. B. Directing the Self-Assembly of Block Copolymers. *Prog. Polym. Sci.* **2007**, *32*, 1152–1204.
4. Bates, F. S.; Fredrickson, G. H. Block Copolymers—Designer Soft Materials. *Phys. Today* **1999**, *52*, 32–38.
5. Bang, J.; Jeong, U.; Ryu, D. Y.; Russell, T. P.; Hawker, C. J. Block Copolymer Nanolithography: Translation of Molecular Level Control to Nanoscale Patterns. *Adv. Mater.* **2009**, *21*, 4769–4792.
6. Li, R. R.; Dapkus, P. D.; Thompson, M. E.; Jeong, W. G.; Harrison, C.; Chaikin, P. M.; Register, R. A.; Adamson, D. H. Dense Arrays of Ordered GaAs Nanostructures by Selective Area Growth on Substrates Patterned by Block Copolymer Lithography. *Appl. Phys. Lett.* **2000**, *76*, 1689–1691.

7. Park, M.; Harrison, C.; Chaikin, P. M.; Register, R. A.; Adamson, D. H. Block Copolymer Lithography: Periodic Arrays of Similar to 10^{11} Holes in 1 Square Centimeter. *Science* **1997**, *276*, 1401–1404.
8. Harrison, C.; Park, M.; Chaikin, P. M.; Register, R. A.; Adamson, D. H. Lithography with a Mask of Block Copolymer Microstructures. *J. Vac. Sci. Technol., B* **1998**, *16*, 544–552.
9. Liu, K.; Baker, S. M.; Tuominen, M.; Russell, T. P.; Schuller, I. K. Tailoring Exchange Bias with Magnetic Nanostructures. *Phys. Rev. B* **2001**, *63*, 060403.
10. Cheng, J. Y.; Sanders, D. P.; Truong, H. D.; Harrer, S.; Friz, A.; Holmes, S.; Colburn, M.; Hinsberg, W. D. Simple and Versatile Methods To Integrate Directed Self-Assembly with Optical Lithography Using a Polarity-Switched Photoresist. *ACS Nano* **2010**, *4*, 4815–4823.
11. Black, C. T. Polymer Self-Assembly as a Novel Extension to Optical Lithography. *ACS Nano* **2007**, *1*, 147–150.
12. Ruiz, R.; Kang, H. M.; Detcheverry, F. A.; Dobisz, E.; Kercher, D. S.; Albrecht, T. R.; de Pablo, J. J.; Nealey, P. F. Density Multiplication and Improved Lithography by Directed Block Copolymer Assembly. *Science* **2008**, *321*, 936–939.
13. Chan, Y. N. C.; Craig, G. S. W.; Schrock, R. R.; Cohen, R. E. Synthesis of Palladium and Platinum Nanoclusters within Microphase-Separated Diblock Copolymers. *Chem. Mater.* **1992**, *4*, 885–894.
14. Forster, S.; Antonietti, M. Amphiphilic Block Copolymers in Structure-Controlled Nanomaterial Hybrids. *Adv. Mater.* **1998**, *10*, 195–217.
15. Moffitt, M.; Eisenberg, A. Size Control of Nanoparticles in Semiconductor-Polymer Composites.1. Control *via* Multiplet Aggregation Numbers in Styrene-Based Random Ionomers. *Chem. Mater.* **1995**, *7*, 1178–1184.
16. Sankaran, V.; Cummins, C. C.; Schrock, R. R.; Cohen, R. E.; Silbey, R. J. Small Pbs Clusters Prepared *via* Romp Block Copolymer Technology. *J. Am. Chem. Soc.* **1990**, *112*, 6858–6859.
17. Peng, Q.; Tseng, Y. C.; Darling, S. B.; Elam, J. W. Nanoscopic Patterned Materials with Tunable Dimensions *via* Atomic Layer Deposition on Block Copolymers. *Adv. Mater.* **2010**, *22*, 5129–5133.
18. Peng, Q.; Tseng, Y. C.; Darling, S. B.; Elam, J. W. A Route to Nanoscopic Materials *via* Sequential Infiltration Synthesis on Block Copolymer Templates. *ACS Nano* **2011**, *5*, 4600–4606.
19. Lin, Y.; Daga, V. K.; Anderson, E. R.; Gido, S. P.; Watkins, J. J. Nanoparticle-Driven Assembly of Block Copolymers: A Simple Route to Ordered Hybrid Materials. *J. Am. Chem. Soc.* **2011**, *133*, 6513–6516.
20. Wei, Q. S.; Lin, Y.; Anderson, E. R.; Briseno, A. L.; Gido, S. P.; Watkins, J. J. Additive-Driven Assembly of Block Copolymer-Nanoparticle Hybrid Materials for Solution Processable Floating Gate Memory. *ACS Nano* **2012**, *6*, 1188–1194.
21. Lopes, W. A.; Jaeger, H. M. Hierarchical Self-Assembly of Metal Nanostructures on Diblock Copolymer Scaffolds. *Nature* **2001**, *414*, 735–738.
22. Zehner, R. W.; Lopes, W. A.; Morkved, T. L.; Jaeger, H.; Sita, L. R. Selective Decoration of a Phase-Separated Diblock Copolymer with Thiol-Passivated Gold Nanocrystals. *Langmuir* **1998**, *14*, 241–244.
23. Zehner, R. W.; Sita, L. R. Electroless Deposition of Nanoscale Copper Patterns *via* Microphase-Separated Diblock Copolymer Templated Self-Assembly. *Langmuir* **1999**, *15*, 6139–6141.
24. Tseng, Y. C.; Peng, Q.; Ocola, L. E.; Czaplewski, D. A.; Elam, J. W.; Darling, S. B. Etch Properties of Resists Modified by Sequential Infiltration Synthesis. *J. Vac. Sci. Technol., B* **2011**, *29*, 06FG01.
25. Johnston, D. E.; Lu, M.; Black, C. T. Plasma Etch Transfer of Self-Assembled Polymer Patterns. *J. Micro/Nanolithogr., MEMS* **2012**, *11*, 031306.
26. Allen, J. E.; Ray, B.; Khan, M. R.; Yager, K. G.; Alam, M.; Black, C. T. Self-Assembly of Single Dielectric Nanoparticle Layers and Integration in Polymer-Based Solar Cells. *Appl. Phys. Lett.* **2012**, *101*, 063105.
27. Tseng, Y. C.; Peng, Q.; Ocola, L. E.; Elam, J. W.; Darling, S. B. Enhanced Block Copolymer Lithography Using Sequential Infiltration Synthesis. *J. Phys. Chem. C* **2011**, *115*, 17725–17729.
28. Gay, G.; Baron, T.; Agraffeil, C.; Salhi, B.; Chevolleau, T.; Cunge, G.; Grampeix, H.; Tortai, J. H.; Martin, F.; Jalaguier, E.; *et al.* CMOS Compatible Strategy Based on Selective Atomic Layer Deposition of a Hard Mask for Transferring Block Copolymer Lithography Patterns. *Nanotechnology* **2010**, *21*, 435301.
29. Mansky, P.; Liu, Y.; Huang, E.; Russell, T. P.; Hawker, C. J. Controlling Polymer−Surface Interactions with Random Copolymer Brushes. *Science* **1997**, *275*, 1458–1460.
30. Knochel, P.; Singer, R. D. Preparation and Reactions of Polyfunctional Organozinc Reagents in Organic-Synthesis. *Chem. Rev.* **1993**, *93*, 2117–2188.
31. Sinha, A.; Hess, D. W.; Henderson, C. L. Transport Behavior of Atomic Layer Deposition Precursors through Polymer Masking Layers: Influence on Area Selective Atomic Layer Deposition. *J. Vac. Sci. Technol., B* **2007**, *25*, 1721–1728.
32. Burkstrand, J. M. Electron Spectroscopic Study of Oxygen-Plasma-Treated Polymer Surfaces. *J. Vac. Sci. Technol.* **1978**, *15*, 223–226.
33. Wade, W. L.; Mammone, R. J.; Binder, M. Surface-Properties of Commercial Polymer-Films Following Various Gas Plasma Treatments. *J. Appl. Polym. Sci.* **1991**, *43*, 1589–1591.
34. Wells, R. K.; Badyal, J. P. S.; Drummond, I. W.; Robinson, K. S.; Street, F. J. A Comparison of Plasma-Oxidized and Photo-oxidized Polystyrene Surfaces. *Polymer* **1993**, *34*, 3611–3613.
35. Choi, J. O.; Moore, J. A.; Corelli, J. C.; Silverman, J. P.; Bakhru, H. Degradation of Poly(methylmethacrylate) by Deep Ultraviolet, X-ray, Electron-Beam, and Proton-Beam Irradiations. *J. Vac. Sci. Technol., B* **1988**, *6*, 2286–2289.
36. Murakami, T. N.; Fukushima, Y.; Hirano, Y.; Tokuoka, Y.; Takahashi, M.; Kawashima, N. Surface Modification of Polystyrene and Poly(methyl methacrylate) by Active Oxygen Treatment. *Colloids Surf., B* **2003**, *29*, 171–179.
37. Kamigaito, M.; Maeda, Y.; Sawamoto, M.; Higashimura, T. Living Cationic Polymerization of Isobutyl Vinyl Ether by Hydrogen-Chloride Lewis Acid Initiating Systems in the Presence of Salts—*In-Situ* Direct NMR Analysis of the Growing Species. *Macromolecules* **1993**, *26*, 1643–1649.
38. Kumar, V.; Dev, S. Titanium Tetrachloride, an Efficient and Convenient Reagent for Thioacetalization. *Tetrahedron Lett.* **1983**, *24*, 1289–1292.
39. Klein, R. J.; Fischer, D. A.; Lenhart, J. L. Systematic Oxidation of Polystyrene by Ultraviolet-Ozone, Characterized by Near-Edge X-ray Absorption Fine Structure and Contact Angle. *Langmuir* **2008**, *24*, 8187–8197.
40. Onyiriuka, E. C. The Effects of High-Energy Radiation on the Surface-Chemistry of Polystyrene—A Mechanistic Study. *J. Appl. Polym. Sci.* **1993**, *47*, 2187–2194.
41. Silverstein, R. M.; Webster, F. X.; Kiemle, D. J. *Spectrometric Identification of Organic Compounds*, 7th ed.; John Wiley & Sons: New York, 2005.
42. Thurn-Albrecht, T.; Steiner, R.; DeRouchey, J.; Stafford, C. M.; Huang, E.; Bal, M.; Tuominen, M.; Hawker, C. J.; Russell, T. Nanoscopic Templates from Oriented Block Copolymer Films. *Adv. Mater.* **2000**, *12*, 787–791.
43. Leskela, M.; Ritala, M. Atomic Layer Deposition Chemistry: Recent Developments and Future Challenges. *Angew. Chem., Int. Ed.* **2003**, *42*, 5548–5554.
44. Gong, B.; Peng, Q.; Parsons, G. N. Conformal Organic−Inorganic Hybrid Network Polymer Thin Films by Molecular Layer Deposition Using Trimethylaluminum and Glycidol. *J. Phys. Chem. B* **2011**, *115*, 5930–5938.
45. Simka, H.; Willis, B. G.; Lengyel, I.; Jensen, K. F. Computational Chemistry Predictions of Reaction Processes in Organometallic Vapor Phase Epitaxy. *Prog. Cryst. Growth Charact. Mater.* **1997**, *35*, 117–149.
46. Ruiz, R.; Wan, L.; Lille, J.; Patel, K. C.; Dobisz, E.; Johnston, D. E.; Kisslinger, K.; Black, C. T. Image Quality and Pattern Transfer in Directed Self Assembly with Block-Selective Atomic Layer Deposition. *J. Vac. Sci. Technol., B* **2012**, *30*, 06F202.